Journal of Biomedical Optics 6(2), 224–230 (April 2001)

Advanced digital photoelastic investigations on the tooth–bone interface

Anand Asundi
Anil Kishen
Nanyang Technological University
School of Mechanical and Production Engineering
Singapore 639798

Abstract. The purpose of this study was to investigate the behavior of the tooth–bone interface on the nature of stress distribution in the tooth and its supporting alveolar bone for various occlusal loads using an advanced digital photoelastic technique. A digital image processing system coupled with a circular polariscope was used for the stress analysis. The phase shift technique and a phase unwrapping algorithm was utilized for fringe processing. This aids in obtaining qualitative and quantitative information on the nature of stress distribution within the dento-osseous structures. The experiments revealed bending stresses within dento-osseous structures. However, the compressive stress magnitude was larger than the tensile stress. Zero stress regions were also identified within the dento-osseous structures. The results suggest that the geometry of the dento-osseous structures and the structural gradients at the tooth–bone interface play a significant role in the distribution of stresses without stress concentrations. Further, the application of an advanced image-processing system with the circular polariscope showed notable advantages and could be applied in other biomechanical investigations. [DOI: 10.1117/1.1344587]

Keywords: digital photoelasticity; phase shifting; stress analysis; tooth–bone interface.

Paper JBO-90060 received Nov. 12, 1999; revised manuscript received May 19, 2000; accepted for publication Dec. 4, 2000.

1 Introduction

It is believed that natural dentition during mastication exhibits a complex pattern of movement in which periodontal ligament (PDL) helps to distribute forces.[1] The classical view for the tooth support mechanism suggests that the PDL is a ''suspensory ligament'' which transmits axial loads in the form of tension to the alveolar bone.[2] However, different *in vivo* experiments[3,4] and electron microscopic studies on the microstructural features of the PDL have shown that the structure of this connective tissue is dictated by the mechanical demands placed on it.[5,6] Previous studies have also concluded that the PDL had features of a connective tissue that are in tension and compression, with more evidence favoring compression.[7,8]

The interface between the tooth and supporting bone or between an implant and bone has been of special concern since they are prone to fail due to overloading of the tooth or the implant.[9] Recent years have seen an increased interest towards regenerating the lost supporting bone with various synthetic biomaterials. This dental biomechanical study utilizes principles of engineering mechanics to obtain deeper understanding on the functional behavior of the tooth–bone system. These studies will provide information on the functional adaptation of the tooth–bone interface and would highlight demands placed on the artificial biomaterials when used during treatment procedures.

Address all correspondence to Anand Asundi, School of Mechanical and Production Engineering, 50 Nayang Ave., Singapore 639798. E-mail: masundi@ntu.edu.sg

Photoelasticity is an established experimental technique that provides whole stress field information.[10,11] However there are various limitations in its past applications in dentistry. Traditionally photoelastic experiments are done to identify regions of stress concentration especially when using mechanical variables such as pins, posts or implants.[12,13] These experiments used scaled up models for testing.[14] The tests required larger than normal occlusal forces to generate sufficient fringes for manual analysis. Finally, previous experiments attempted to simulate the geometry of the structures only. No attempt was made to consider the relative modulus difference between different dental structures.[10,15]

In this study we utilize an image-processing system along with the circular polariscope for stress analysis. The present system facilitates experimentation of miniature models with enhanced sensitivity and accuracy. Further, the fringe processing method (phase shift technique) utilized in this investigation cannot only analyze complex fringe patterns, but can also identify signs of the fringe orders.[16] All the above helps in attaining an improved understanding of the nature of stress distribution within dento-osseous structures.

2 Materials and Methods

2.1 Model Preparation

A human mandible with dentition, obtained from a male adult cadaver, was sectioned vertically along the symphysis region. These sections were digitized using an image-processing sys-

1083-3668/2001/$15.00 © 2001 SPIE

tem and the coordinates were measured. These coordinates were then utilized by a computer numerical control (CNC) machine to fabricate sectional epoxy models of the lower central incisor tooth and supporting mandibular bone. This process of machining used to prepare photoelastic models resulted in no residual stresses in the models when examined in a polariscope.

Models were prepared based on the relative modulus of elasticity of the anatomical dento-osseous structures. Photoelastic sheets 254×254 mm^2, with thickness of 3.20 mm and Young's modulus of 2.5 GPa were used to prepare the models. A layer of chemically cured silicon rubber, 0.35 mm thick and an elastic modulus of 0.2 MPa, was used to simulate the periodontal ligament. A specially manufactured polyester reinforced composite sheet 0.15 mm thick simulated the root cementum. This sheet had an elastic modulus that was similar to that of the epoxy model but with higher resilience. The above thickness for silicon rubber and polyester reinforced composite sheet was chosen so as to simulate the original anatomical dimensions of the periodontal ligament and cementum layer, respectively. A dental composite with a Young's modulus of 13.6 GPa was used to fabricate the enamel portion of the model.

2.2 Experimental Arrangement

The experimental setup consisted of a standard circular polariscope, a charge coupled device (CCD) camera and a digital computer [Figures 1(A) and 1(B)]. The CCD camera and the digital computer, which constitute the image-processing system, are for acquisition and analysis of the fringe patterns.

A special loading device was fabricated that could hold anatomical sized models. A load cell was placed on the superior part of the loading device. This was for measuring the applied load. The loading device had individual slots that could direct loads along the long axis (0°) and 60° lingual to the long axis of the tooth. The angles were chosen to simulate forces applied in different biting conditions.

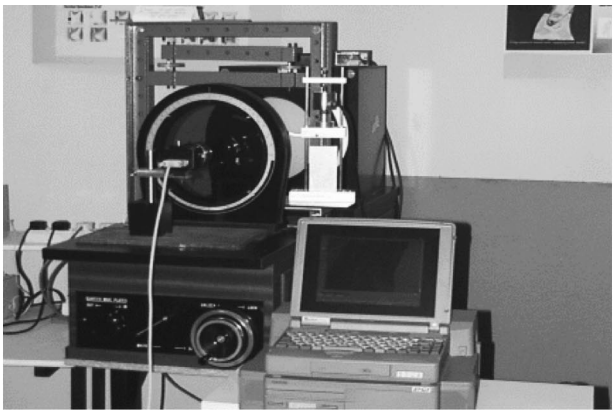

(a)

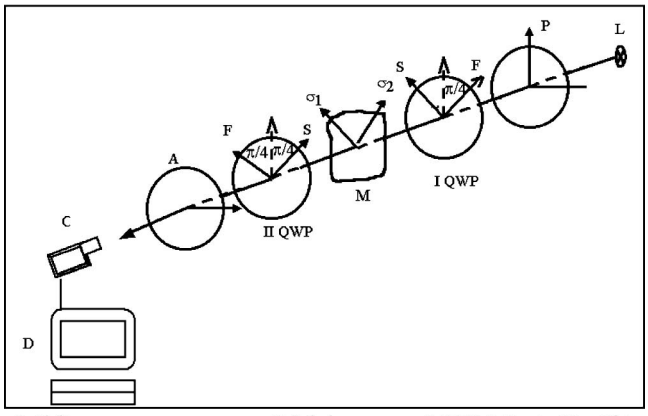

(b)

Fig. 1 (A) Experimental arrangement. (B) Schematic of the experimental setup, showing various components of the circular polariscope and the digital image-processing system.

2.3 Experiments

The experiments were divided into two stages. The first stage experiment was done with model 1. This model simulates a normal tooth and supporting bone with periodontal ligament and cementum at their interface. These experiments were done to investigate the nature of stress distribution within the tooth structure.

The second stage of the experiments used models 2, 3 and 4. These three models were categorized on the basis of materials used at the tooth–bone interface. Model 2 simulated only the PDL at the interface. Model 3 simulated the PDL and cementum at the interface. Model 4 was used as a control with no PDL or cementum. In this model plasticine was used at the tooth–bone interface as a filler material with no elastic property. Six models were prepared for each of the four groups.

Each group of models was tested at 25, 55, 125, 150 and 200 N loads applied along the long axis of the tooth (0°) and 60° lingual to the long axis of the tooth. The fringe patterns obtained during the experiments were acquired by the CCD camera and were stored in the digital computer. During each experiment four phase-shifted images were recorded by rotating the analyzer by angles of 0°, 45°, 90° and 135° with respect to the axis of the polarizer. Each test was repeated three times to reconfirm the repeatability.

2.4 Digital Stress Analysis

The stress optic law is given as

$$\sigma_1-\sigma_2=\frac{\theta}{2\pi}\,\frac{f_\sigma}{h}=\frac{Nf_\sigma}{h}, \tag{1}$$

where $(\sigma_1-\sigma_2)$ is the difference in the in-plane principal stress, f_σ is the material fringe value, h is the thickness of the specimen, $\theta/2\pi$ is the resultant optical phase generated due to the stress-birefringence in the model and $N(=\theta/2\pi)$ is the fringe order assigned to the dark fringes. In the traditional dark-field polariscope these fringes are counted manually and assigned a non-negative integer.[17] In the present study a phase shifting method is developed for the calculation of phase, and thus the fringe order, at every point of interest.

The fringe intensity (I_x) at any point in the model is given as

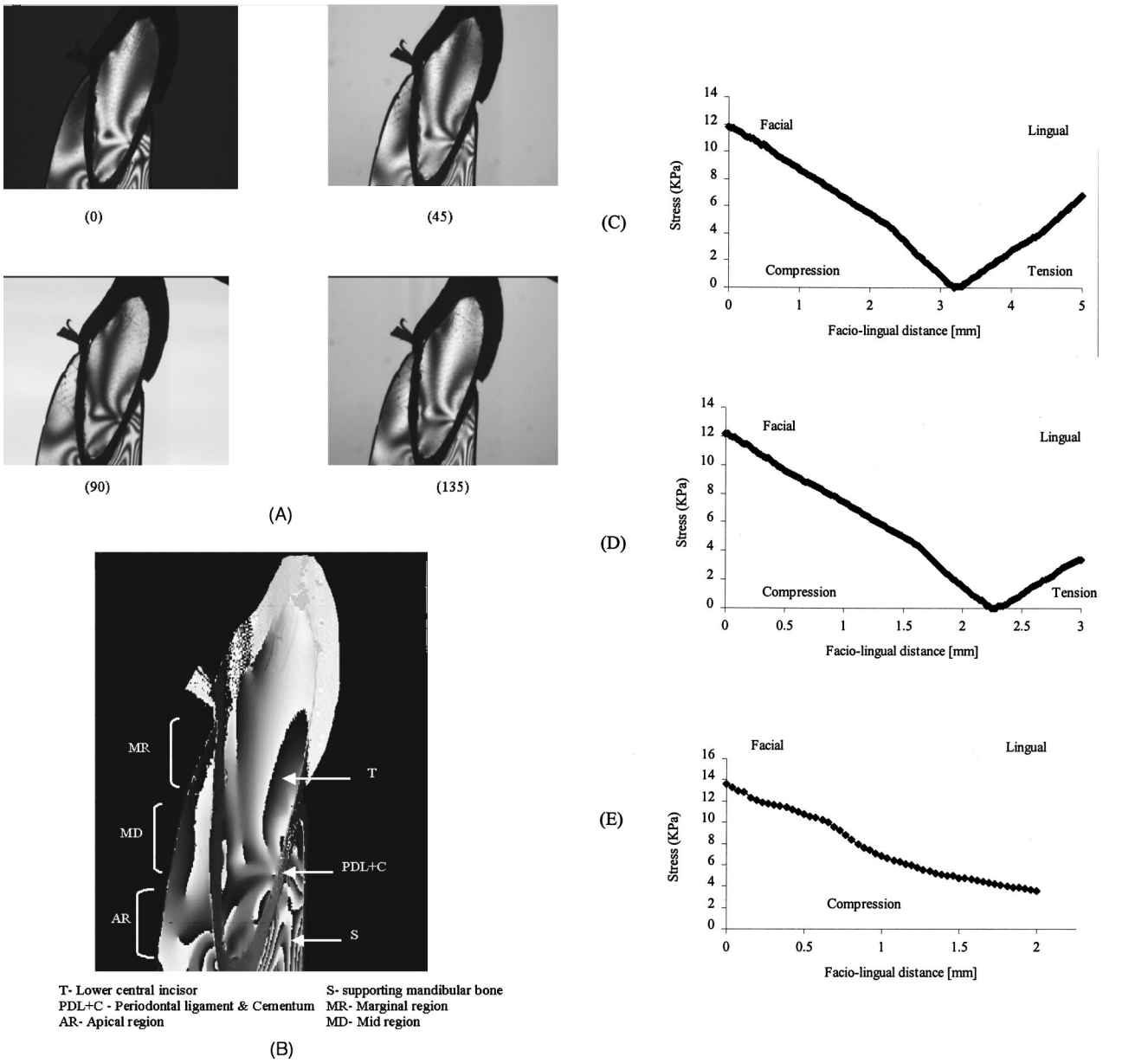

Fig. 2 (A) Isochromatic fringe patterns acquired for model 1 (a normal tooth) at four phases by rotating the analyzer 0°, 45°, 90° and 135° with respect to the polarizer. Model 1 was loaded at 150 N, along the long axis. (B) Phase wrapped image obtained from the four phase-shifted images in (A), for model 1. (C) Graph showing the stress distribution pattern in the cervical third of the root for model 1 (a normal tooth). A 150 N load was applied along the long axis. (D) Graph showing the stress distribution pattern in the middle third of the root for model 1 (a normal tooth). A 150 N load was applied along the long axis. (E) Graph showing the stress distribution pattern in the apical third of the root for model 1 (a normal tooth). A 150 N load was applied along the long axis.

$$I_x = I_b + I_0 \cos(\theta_x + \alpha), \tag{2}$$

where I_b is the mean intensity of the pattern, I_0 is the amplitude of the fringe pattern, α is a known added phase and θ_x is the required phase at the point. Adding four equal phase steps (α) between 0 and π generates phase-shifted images. From the intensities I_1, I_2, I_3 and I_4 of these four phase-shifted images the fringe orders at every point (N_x) are calculated as[16]

$$\frac{\theta_x}{2\pi} = N_x = \frac{1}{2\pi} \tan^{-1} \frac{I_4 - I_2}{I_1 - I_3}. \tag{3}$$

In our experiment, rotating the analyzer 0°, 45°, 90° and 135° with respect to the polarizer induces the required phase steps. These four phase-shifted images [Figure 2(A)] are evaluated using Eq. (3) to obtain a wrapped phase map [Figure 2(B)].[17] The stress distribution pattern obtained from the wrapped phase map is similar to that of the conventional method. Here the stress patterns displayed a sequential increase in distribution. They did not provide any information on the nature or direction of distribution. Hence phase unwrapping was done along select lines in the wrapped image to make the fringe modulation continuous and to provide information on the direction and magnitude of the stress distribution. The phase

unwrapping method is based on modulation ordering and relies on the intensity modulation in pixels. A circular calibration disk was analyzed to calibrate and confirm the accuracy of the system (material fringe coefficient=6.825 K Pa/fringe/m).[18]

3 Results

3.1 Stage I: Stress Distribution Within the Tooth

3.1.1 *Model 1: Normal Tooth and Supporting Bone*

Figure 2(A) shows the four phase-shifted isochromatic fringe patterns for model 1, at 150 N load, applied along the long axis of the tooth. Figure 2(B) shows the wrapped phase image obtained from the four phase-shifted images. Unwrapping reveals patterns characteristic of bending stresses at the cervical region [Figure 2(C)] and midregion of the root [Figure 2(D)], indicated by compressive stresses on the facial side and tensile stresses on the lingual side. The magnitude of compressive stress on the facial side is significantly higher than the tensile stress on the lingual side. There is a reduction in the bending stresses towards the apical region, with only compressive stress in the apical third of the root [Figure 2(E)]. A zero order fringe is also identified within the tooth.

3.2 Stage II: Behavior of the Tooth–Bone Interface and Stress Distribution Within the Alveolar Bone

3.2.1 *Model 2: Simulated PDL at the Interface*

Figure 3(A) depicts the isochromatic fringe pattern for a load of 125 N, directed along the long axis of the tooth. There is compression in the supporting bone model exerted by the tooth model at the midregion of the facial supporting bone and at the apical region of the lingual supporting bone. The stress distribution patterns in the midregion of the facial supporting bone and the apical region of the lingual supporting bone are shown in Figures 3(B) and 3(C), respectively. The apical region of the facial supporting bone shows a bending stress pattern, with higher compressive stress in comparison to the tensile stress [Figure 3(D)]. A zero stress region is identified in the supporting bone near the root apex.

At higher loads there is a concentration of stress at the apical region of the lingual supporting bone and at the midregion of the facial supporting bone. However the zero order fringe in proximity to the root apex persisted even for higher loads. The marginal region of the facial supporting bone is found to be relatively unstressed for different loading conditions.

3.2.2 *Model 3: Simulated PDL and the Cementum at the Interface*

Figure 4(A) shows the isochromatic fringe pattern for model 3 at a load of 125 N, when directed along the long axis of the tooth. It is observed from these experiments that the major stresses from the tooth root surface are distributed to the supporting bone primarily along the marginal region of the facial supporting bone [Figure 4(B)] and from the apical region of the lingual supporting bone [Figure 4(C)]. These regions show a relatively constant magnitude of stress.

Stresses occur predominantly on the facial supporting bone in comparison to on the lingual surface. Significant bending stress patterns are noticed on the supporting bone model on the middle and apical regions of the facial supporting bone [Figure 4(D)]. A zero order fringe is identified in the supporting bone model near the root apex. There is no significant stress concentration along the entire specimen for loads ranging from 25 to 170 N. However at 200 N the stresses at the apical region of the lingual supporting bone showed a tendency to concentrate. The zero order fringe in the supporting bone near the root apex persists even at higher loads.

3.2.3 *Model 4: No PDL or Cementum at the Interface*

Figure 5(A) displays the isochromatic fringe patterns for model 4 at 50 N load. It is identified that stresses are substantially concentrated in the midregion of the facial supporting bone and apical region of the lingual supporting bone. The stress distribution patterns in the midregion of the facial supporting bone and apical region of the lingual supporting bone are shown in Figures 5(B) and 5(D), respectively. The marginal region of the supporting bone is relatively unstressed. A stress pattern characteristic of bending is observed at the apical region of the facial supporting bone, with higher compressive stress distributed in comparison to tensile [Figure 5(C)]. Further, it is also noticed that, as the load increases, the zero stress order fringe in the supporting bone associated with the root apex tends to move away from the root tip.

4 Discussion

The present application of a digital image-processing system along with the circular polariscope had distinct advantages. The high resolution CCD camera used in this system enabled testing of anatomical sized models. Further, the four step phase shift technique utilized in this study for fringe processing was not only sensitive to minimal occlusal loads but it also had an important advantage of identifying the direction of increasing and decreasing fringe orders. This facilitated experimental analysis of complex photoelastic fringe patterns like those observed in biological specimens.

The first stage of experiments was conducted to understand the nature of stress distribution within the tooth for occlusal loads directed along the long axis and at 60° lingual to the long axis of the tooth. It was found that the tooth showed significant bending stress in the cervical and midregion of the root. The bending stress distribution in the engineering structure results when a columnar structure is subjected to an eccentric load [i.e., loads acting away from the line of symmetry as shown in Figure 6(C)]. The column tends to bend, resulting in compressive stress on one side and tensile stress on the other side. These stresses are highest at the borders and diminish to zero towards the middle of the cross section [Figure 6(B)]. The bending stresses [Figure 6(B)] coupled with the compressive axial stress [Figure 6(A)] give the resulting stress distribution seen in Figure 6(C), showing higher compressive stresses compared to tensile stresses. In the tooth, as with the eccentric loading, the compressive stresses along the facial surface were substantially higher in comparison to the tensile stresses along the lingual side of the root. This increased propensity toward compressive stresses in comparison toward

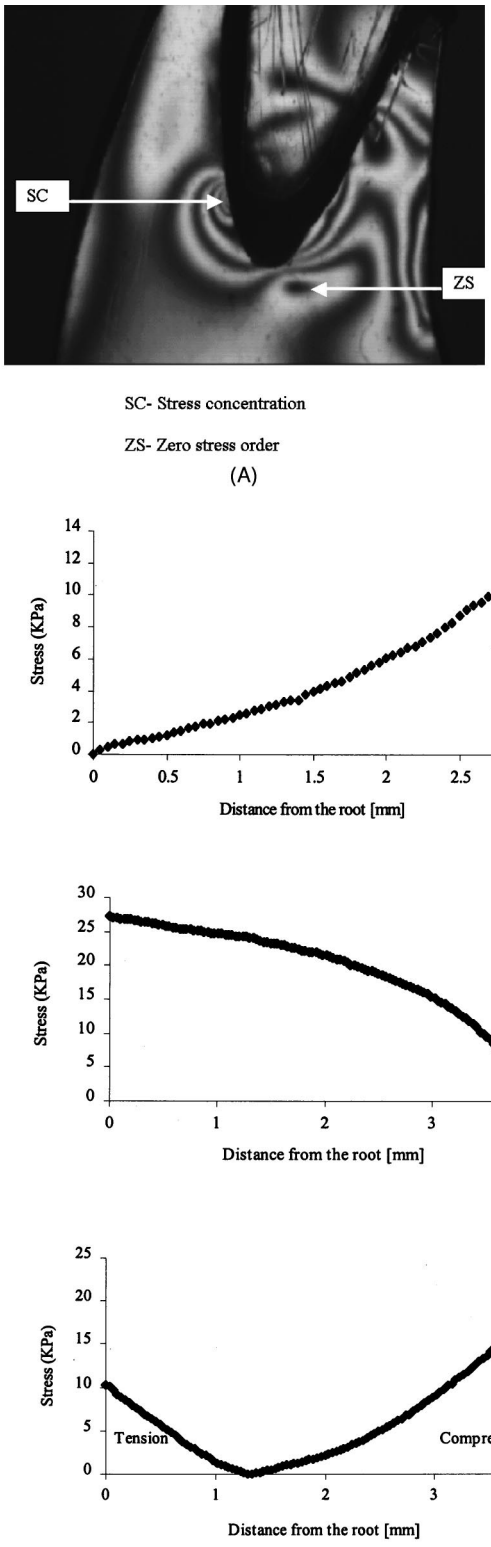

Fig. 3 (A) Isochromatic fringe patterns for model 2 that simulated the PDL. A 125 N load was applied along the long axis of the tooth. (B) Graph showing the stress distribution pattern for model 2 (simulated PDL) in the midregion of the facial supporting bone. The applied load was 125 N, directed along the long axis. (C) Graph showing the stress distribution pattern for model 2 (simulated PDL) in the apical region of the lingual supporting bone. The applied load was 125 N, directed along the long axis. (D) Graph showing the stress distribution pattern for model 2 (simulated PDL) in the apical region of the facial supporting bone. The applied load was 125 N, directed along the long axis.

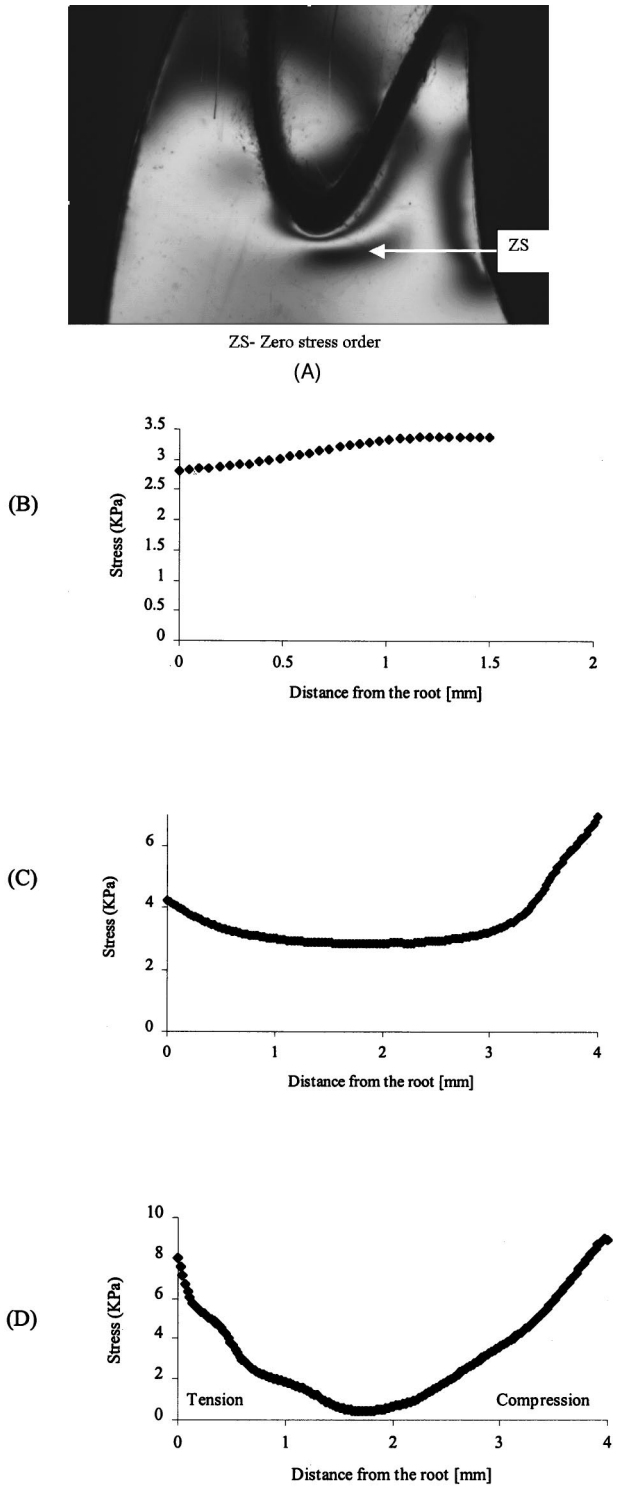

Fig. 4 (A) Isochromatic fringe patterns for model 3 that simulated the periodontal ligament and cementum. A 125 N load was applied along the long axis of the tooth. (B) Graph showing the stress distribution pattern for model 3 (simulated PDL and cementum) in the marginal region of the facial supporting bone. The applied load was 125 N, directed along the long axis. (C) Graph showing the stress distribution pattern for model 3 (simulated PDL and cementum), in the apical region of the lingual supporting bone. The applied load was 125 N, directed along the long axis. (D) Graph showing the stress distribution pattern for model 3 (simulated PDL and cementum), in the apical region of the facial supporting bone. The applied load was 125 N, directed along the long axis.

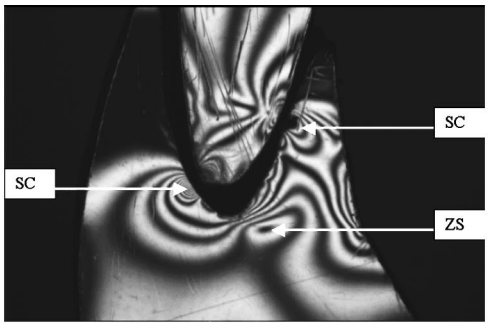

SC- Stress concentration

ZS- Zero stress order

(A)

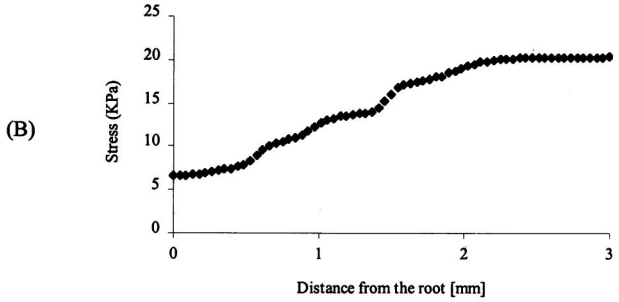

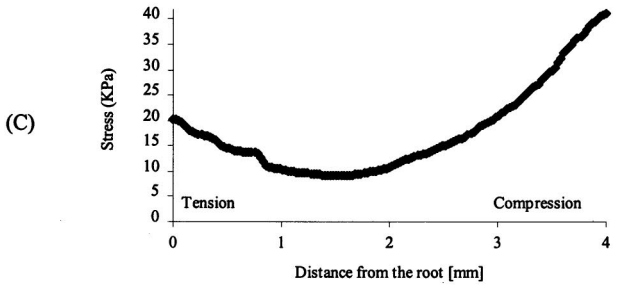

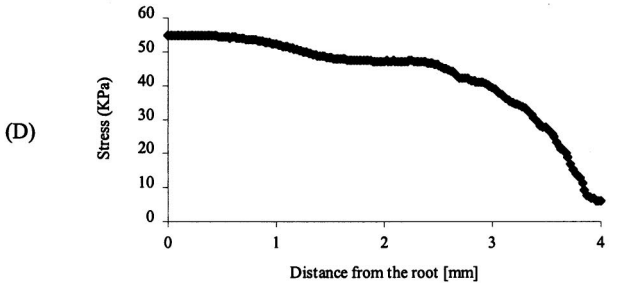

Fig. 5 (A) Isochromatic fringe patterns for model 4, with no periodontal ligament and cementum. A load of 50 N was applied along the long axis of the tooth. (B) Graph showing the stress distribution pattern for model 4 (no PDL and cementum) in the midregion of the facial supporting bone. The applied load was 50 N, directed along the long axis. (C) Graph showing the stress distribution pattern for model 4 (no PDL and cementum) in the apical region of the facial supporting bone. The applied load was 50 N, directed along the long axis. (D) Graph showing the stress distribution pattern for model 4 (no PDL and cementum) in the apical region of the lingual supporting bone. The applied load was 50 N, directed along the long axis.

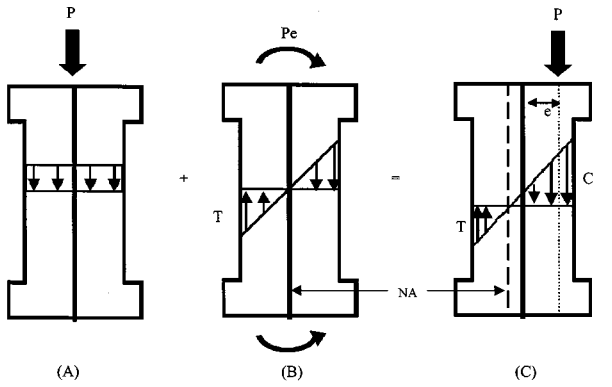

P- Load Pe- Bending moment C- Compression T- Tension NA- Neutral axis along which stress is zero e- distance of the load from the axis of symmetry

Fig. 6 Schematic diagrams showing the nature of stress distributions in a column. (A) Distribution of compressive stress when a load is applied along the axis of symmetry. (B) Distribution of bending stress when a bending moment is applied. Bending stress resulted in compressive stress on one side and tensile stress on the other with a neutral stress plane intervening. (C) Distribution of bending stress when a load is applied at a distance *e* from the axis of symmetry. This resulted in higher compressive stress than tensile stress.

tensile was due to the shape and angulation of the tooth and supporting bone reactions rather than the eccentricity of loading (Figure 7). Further, the apical region of the root showed a notable reduction in bending and manifested particularly compressive stress.

In our experiments the compressive stresses and tensile stresses identified during bending were reconfirmed using the fingernail test.[19] This test suggests that if the edge of the model is pressed with a finger or the thumb nail, compression and tensile fringes react in a distinct manner, enabling them to

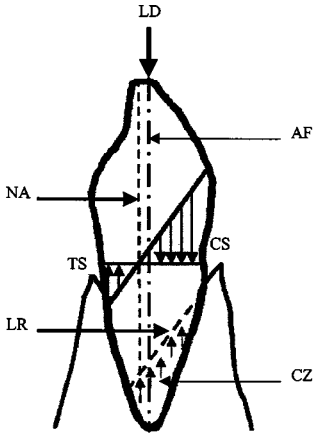

LD- Load
CS- Compressive stress
TS- Tensile stress
NA- Neutral axis along which stress is zero
CZ- Compressive zone
AF- Axis of force
LR- Line resulting from the reactant stresses produced by the initial contact of tooth with supporting bone.

Fig. 7 Schematic illustration of the bending stress distribution within the tooth (model 1).

be distinguished. If the boundary stress is compressive then the fringes are drawn towards the boundary and if the boundary stress is tensile the fringes moves away from the boundary.

The second stage of experiments was done to study the behavior of the tooth–bone interface and the nature of stress distribution within the dental supporting bone. The supporting bone exhibited predominant bending stress patterns. However it was identified that the compressive stresses dominated over the tensile stresses. It was also noticed that the model that simulated major anatomical features such as dentine, alveolar bone proper, periodontal ligament and cementum had a unique distribution of stresses without undue stress concentrations. These experiments showed that the structural gradients were significant in distributing stresses at the tooth–bone interface.

The models prepared and used in the present investigations were based on the relative elastic modulus of the major anatomical structures and it should be noted that the elastic modulus within a specific biological structure such as dentine is not homogeneous. Yet this modeling technique is used so as to appreciate the hypothesis that dental tissues originate as homogeneous structures that adapt to functional forces. Furthermore, fluoroscopic x-ray microscopic image analysis on the tooth sections revealed a significant congruence between the nature of stress distribution in the normal tooth (model 1) and the pattern of mineralization within the human dentine.[20] These findings substantiate the aforementioned hypothesis that dental tissues are biologically adaptive structures.

It was observed during the entire second stage of our analysis that the cervical root region on the facial side and the apical root region on the lingual side made primary contact with the supporting structures during loading. Previous studies[21] have suggested that the cementum thickness was not uniform throughout but exhibited a ''site-specific'' maximum. In this observation the mandibular incisor had a maximum width root cementum on the lingual aspect of the apical root and on the facial aspect cervically, which coincided with the regions in our experiments where the root surface made initial contact with the supporting bone. Also, experimental analysis performed in model 1 and model 2 showed that the PDL primarily distributed stresses from the upper root surface, while the cementum layer prevented stress concentrations and distributed compressive stresses to the supporting bone. This could be the reason for the threefold increase in the active apical cementum layer with age.[22]

Acknowledgement

The support of Nanyang Technological University through research Grant No. MLC1/97 is acknowledged.

References

1. F. A. Carranza, *Clinical Periodontology* (Saunders, Philadelphia, 1990), pp. 71–73.
2. E. L. DuBrul, *Oral Anatomy* (Ishiyaku EuroAmerica, St. Louis, 1990), p. 136.
3. D. C. Picton and W. I. R. Davies, ''Dimensional changes in the periodontal membrane of monkeys (Macaca iris) due to horizontal thrust applied to the teeth,'' *Arch. Oral Biol.* **12**, 1635–1643 (1967).
4. D. C. Picton, ''The effect of the intrusive tooth mobility of surgically removing the cervical periodontal ligament in monkeys (Macaca fascicularis),'' *Arch. Oral Biol.* **33**, 301–304 (1988).
5. D. C. Picton and D. J. Willis, ''Visualisation by scanning electron microscopy of the periodontal ligament *in vivo* in the macaque monkey,'' *Arch. Oral Biol.* **26**, 821–825 (1981).
6. M. H. Flint, A. S. Craig, H. C. Reilly, G. C. Gillard and D. A. D. Parry, ''Collagen fibril diameters and glycosaminoglycans content of skins-indices of tissue maturity and function,'' *Connect. Tissue Res.* **13**, 69–81 (1984).
7. M. J. Merrilees and M. H. Flint, ''Ultra structural study of tension pressure zones in a rabbit flexor tendon,'' *Am. J. Anat.* **157**, 87–106 (1980).
8. B. K. B. Berkovitz, M. E. Weaver, R. C. Shore and B. J. Moxhan, ''Fibril diameters in the extra cellular matrix of the periodontal connective tissues of the rat,'' *Connect. Tissue Res.* **8**, 127–132 (1981).
9. W. L. Kydd and C. H. Daly, ''Bone-titanium response to mechanical stress,'' *J. Prosthet. Dent.* **35**, 567–571 (1976).
10. I. Glickman, F. W. Roeber, M. Brion, and J. H. Pameijer, ''Photoelastic analysis of internal stresses in the periodontium created by occlusal forces,'' *J. Periodontol.* **41**, 30 (1970).
11. A. A. Caputo and J. P. Standlee, *Biomechanics in Clinical Dentistry*, pp. 185–203, Quintessence, Chicago (1987).
12. R. G. Craig, M. K. El-Ebrashi, P. J. LePeak, and F. A. Peyton, ''Experimental stress analysis of dental restorations. I. Two-dimensional photoelastic stress analysis of inlays,'' *J. Prosthet. Dent.* **17**, 292–302 (1967).
13. K. C. Rolf, M. W. Parker, and G. B. Pelleu, ''Stress analysis of five prefabricated endodontic dowel designs: A photoelastic study,'' *Oper. Dent.* **17**, 86–92 (1992).
14. J. A. Hood, J. W. Farah, and R. G. Craig, ''Modification of stresses in alveolar bone induced by a tilted molar,'' *J. Prosthet. Dent.* **34**, 415–421 (1975).
15. D. N. Deines, J. D. Eick, C. M. Cobb, C. Q. Bowles, and C. M. Johnson, ''Photoelastic stress analysis of natural teeth and three osseo-integrated implant designs,'' *Int. J. Periodontol. Restorative Dent.* **13**, 540–549 (1993).
16. A. Asundi, ''Phase shifting in photoelasticity,'' *Exp. Tech.* **17**, 19–23 (1993).
17. G. O. Rosvold, ''Fast measurement of phase using a PC-based frame grabber and phase stepping technique,'' *Appl. Opt.* **29**, 237–241 (1990).
18. J. W. Dally and W. F. Riley, *Experimental Stress Analysis*, pp. 425–429, McGraw–Hill, New York (1991).
19. E. J. Hearn, *Photoelasticity*, pp. 20–21, Merrow, England (1971).
20. A. Kishen, U. Ramamurty, and A. Asundi, ''Experimental studies on the nature of property gradients in the human dentine,'' *J. Biomed. Mater. Res.* **51**, 650–659 (2000).
21. H. E. Schroeder, *The Periodontium*, pp. 26–32, Springer, Berlin (1986).
22. H. A. Zander and B. Hurzler, ''Continuous cementum apposition,'' *J. Dent. Res.* **37**, 1035 (1958).